Optica Applicata, Vol. LIII, No. 4, 2023
DOI: 10.37190/oa230404

Study, simulation and detection of glucose concentrations through a biochip based on two-dimensional photonic crystals

Mourad BELLA[1], Mehdi GHOUMAZI[2, *], Ghania SLIMANI[3, 4], Djamel BENATIA[3]

[1]Abdelhafid Boussouf University Center, Mila, Algeria

[2]Non-linear Optics and Optical Fiber Team (ONLFO), Research Unit in Optics and Photonics (UROP), Center for the Development of Advanced Technologies (CDTA), University of Setif-1, 19000 Setif, Algeria

[3]Laboratoire d'Electronique Avancée (LEA) Electronic Department, Faculty of Technology, Batna 2 University, Algeria

[4]Mechanics Research Center (CRM), Chaab Erssas Campus, Mentouri 1 Brothers University, Constantine, Algeria

[*]Corresponding author: mghoumazi@CDTA.DZ

A biochip is made from a two-dimensional photonic crystal waveguide and a rhombus shape that acts as a resonator. This biochip is a sensor that can detect different concentrations of glucose with amounts of 10, 20 and 60% in water. Here, we studied and simulated the concentrations of glucose, which have a refractive index n of 1.3477, 1.3635 and 1.4394, respectively. To identify these quantities, we have proposed a square lattice structure formed by silicon rods with a $n = 3.46$. With the help of these dielectric rods immersed in the air, it was possible to analyze the detection characteristics. Our results are examined according to COMSOL software by using the PWE method and the finite element method in order to have the PBG and which helped us to create the structure and extract the propagation at resonance, the field norm, the total energy density (TED), the power flow norm (PFN), the transmission and the sensitivity. The concentrations of glucose in water answered yes to the variations for each of the E-field, the TED, the PFN and the sensitivity. These variations are due to the radius r and refractive index n of each concentration used. This structure can help with diabetes self-monitoring.

Keywords: photonic crystals, pwe, biochip, glucose, diabetes.

1. Introduction

In 1962, Lyons and Clark, two researchers, invented the first optical sensor. This sensor in turn has opened up to optical detection mechanisms and dreew great attention in several fields such as: the military, environmental monitoring, viscosity and surface tension, medical diagnostics and control of industrial processes, *etc*. One of the mate-

rials that can be detected through the optical sensor is glucose. This material has a concentration that is affected by the physical properties of viscosity, surface tension, specific gravity, and refractive index. Glucose plays an important role in the field of health, for example, in the case of diabetes where its concentration in the urine can infect the patient's condition. Once the glucose level rises in the urine from the normal range, which is between 0 and 15 mg/dl, it is called *glycosuria* which represents its high level in the blood, knowing that normal blood sugar takes the interval between 165 and 180 mg/dl and when the level is too low, it is known as *hypoglycemia* which means a lower range of 40 mg/dl. On one hand, if the interval varies between 270 and 360 mg/deal, it means high blood sugar is known as *hyperglycemia* [1]. Another example of the proper functioning of the body is the monitoring of the level of glucose in the blood, because its presence in the blood is in the form of a fundamental segment for the capacity of vitality, typical functioning of neurons and guide of metabolic exercises. Various techniques have been used to decide on the quantitative and subjective examination of the level of glucose in body fluid. Hence, they are various current sensors, like pyroelectric sensor, piezoelectric sensor, electrical sensor, and optical sensor. Knowing that among the optical sensors there is one that is used in the localization of blood fluid glucose with the purpose of shielding against electromagnetic interference (EMI) with light, high sensitivity and high accuracy [2]. Now, in order to develop ultra-compact optical sensors, different nano- and micrometer photonic structures have been used, such as optical decoders based on photonic crystal (PhC) [3], Mach–Zehnder interferometers (MZI) [4],electro-optical encoders based on PhC [5], surface plasmon resonators [6], micro-ring resonators [7, 8], ultra-compact ultra-fast comparator based on PhC [9] and photonic crystal (PhC) cavities [10]. In order to use them as sensors, it is desirable to have PhC resonators with intense light/matter interaction between analyst and optical fields. These PhC resonators are structures reported by different researchers for detection purposes [11-18]. These resonator structures are most widely used as the ring cavity, which is very sensitive to IR variation and provides better sensitivity compared to other optical devices. Micro-ring resonators (MRR) have high transmission efficiency and high quality factors and small mode volume. PhC resonators can introduce unique advantages in sensing applications to design different biomedical, chemical sensors, *etc*. Photonic crystal sensors (PhC resonators) have sparked critical interest in integrated sensing and the principle of cavity sensors [19] is based on the variation of the properties of the light whose refractive index (RI) of the analyst varies. In this case, optical detection is the current interest that can give both fast reaction and accurate continuous identification of substances [20]. In addition, the refractive index is among the relevant parameters for detection because its modification can infect the electromagnetic modes that come from different frequencies in the photonic forbidden band (BPG). By creating defects at the level of the structure by the omission of rods or holes such as the case of phonic crystals, the radiation will be allowed to travel within the BIP at the recurrence of the deformation [21]. PhCs are periodic structures classified into one-dimensional (1D), two-dimensional (2D) and three -dimensional (3D) with the ability to control the propagation of electromagnetic (EM)

waves in frequency intervals called PBG (photonic band gaps). The creation of the photonic band gap is related to the contrast of refractive index n between the constituent materials [22]. In order to locate refractive index [23], high temperature [24], bio-sensing applications [25], pressure [26], force/strain sensor [27], breast cancer [28]. The proposed 2D-PhC structure is simple, small in size with high light confinement, and more convenient compared to one-dimensional and three-dimensional PhC. Thanks to this high confinement of light inside the device, our design will provide an accurate detection platform. Generally, the photonic crystal has a photonic band gap that can be broken by the creation of a point defect or by a line defect. Several optical devices based on PhCs have been reported by breaking defects such as: demultiplexer [29], switches [30], directional coupler [31], power splitter [32], logic gates [33], triplexer [34], electro-optical modulators [35], add-drop filter [36], filter [37], and sensors [38].

A new technique for detection is proposed for a silicon (Si) based biochip. It uses two-dimensional (2D) photonic crystals to detect changes in the refractive index (RI) of various percentages of glucose concentration in water. The proposed platform is a PhC-2D structure. It is designed with 21×25 air-immersed silicon rods. A rhombus shape at the heart of this design was created by omitting a few rods. In addition, of the two waveguides at the ends of this rhombus are introduced by omitting some rods along the Γ-X direction. Thanks to this defect that we created, the photonic crystals are in a position to control the propagation of light within the structure. This defect plays a key role in detection applications. The distance between each rod is known by the dielectric constant a which is 523 nm. The refractive index n of rods plus air is 3.46 and 1, respectively. Moreover, the radius of the rods r in the initial structure is $0.19a$ which means 99.37 nm. Due to the simplicity, *i.e.* small size and shape as well as the strong confinement of light at the heart of the device which gives them a well-defined and precise detection platform, photonic crystals are the best answer to this field [39]. Furthermore, other sensors based on photonic crystals (PhCs) or based on circular rings based on PhC called (PhCRR) have been used for biodetection applications [40], temperature sensors [41], detection of cancer [42], chemical sensors [43], *etc*.

In this study, a photonic crystal was designed to be based on a biosensor. Therefore, for this we presented the detection characteristics such as the photonic band gap for the TM mode, the distribution of the dielectric constant ε_r along the structure, the electric field norm E with the lattice at resonance (before and after changes in on the radius of the rods) as well as for the following glucose concentrations, 10%, 20%, and 60% in water within the structure. Next, we illustrated the total energy density, power flow norm, and transmission for the proposed glucose concentrations. Our numerical simulation results are obtained using MATLAB and COMSOL software.

2. Materials and methods

Several strategies exist, such as the finite difference method (FDTD), the finite volume method, the finite element method (FEM) [44], and the plane wave expansion (PWE) method [45]. In each method, there are certain disadvantages and advantages.

First, FEM and PWE are particularly used because of their efficiency, which meets the requirements of PC-based devices. Then, the use of the PWE could offer the theoretical analysis of the photonic crystal structures and the eigenmodes at the heart of the periodic structures because it illustrates a superposition of a group of plane waves. And finally, one of the approaches used is the resolution of Maxwell's equations (EM) in order to estimate both the propagation of the electric field (EM) and the transmission via the FEM method.

In this study, the numerical results are obtained using the finite element method (FEM) under COMSOL software [46] and the PBG was calculated by the PWE method. In a first place, we studied and illustrated a two-dimensional square lattice structure based on silicon (Si) photonic crystals immersed in air. Within this structure, a rhombus sandwiched between two horizontal waveguides is formed. These guides represent a line defect that is used to manipulate the propagation of light. The impact of the defect created (point or line) to design the proposed sensor is observed on the photonic forbidden band (PBG). It in turn breaks allowing the guided modes to propagate inside this PBG region. Guided modes are regulated by controlling the shape and size of the defect [47]. In addition, the resonant wavelength, total energy density and power flow norm of the sensor can be changed by varying the refractive index (RI). The electromagnetic equations of Maxwell (1) used can prove that the functions of a photonic crystal are similar to those of the sensor [48].The radius r of the rod is 0.09937 µm, as it remains the same throughout the structure with a lattice constant, a which equals 0.523 µm.

$$\nabla \times \left[\frac{1}{\varepsilon(\mathbf{r})} \times H(\mathbf{r}) \right] = \left(\frac{\omega}{c} \right)^2 H(\mathbf{r}) \tag{1}$$

where c, ε, H and ω represent, the speed of light, the permittivity, the magnetic field and the resonant frequency, respectively. Photonic band gap (PBG) extraction uses

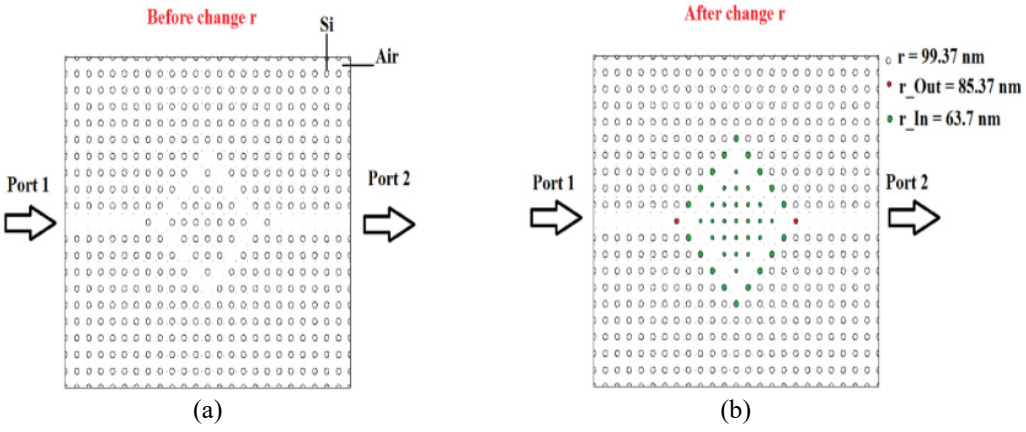

Fig. 1. (a) The initial proposed structure before changing the rods, and (b) after changing the rods.

plane wave expansion (PWE) method which can be implemented to study the dispersion behavior of photonic crystals and transmission spectra. The element method implemented in COMSOL software was used to get the distribution of the dielectric constant ε_r on the structure and its mesh, the propagation at resonance of the electric field norm at different concentrations of glucose (10%, 20% and 60%) in water, the total energy density (TED), power flow norm (PFN) and transmission (T). The proposed sensor based on photonic crystals is useful for detecting the three concentrations of glucose in water. Therefore, the creation of this structure is done by photonic crystal rods on a 2D dimension. It extends towards the *X* direction (horizontally) with 25 rods and towards the *Y* direction (vertically) with 21 rods, forming a square network of 21×25. We know that the rods are immersed in air and the lattice constant *a* of the lattice is 0.523 μm.

In addition, the two refractive indices of silicon rods and air are 3.46 and 1, respectively, and the radius of the rods at CPh without defects (perfect) is 99.37nm, calculated according to the following relationship:

$$r = 0.19a \tag{2}$$

In order to create the rhombus shape at the heart of the two-dimensional structure, we cut some rods and for the guide by removing some rods also along the *Γ*-*X* direction. That is to say, we created defects that are the cause of the control of light inside the proposed design. This defect is used as an application for detection [49].

3. Results and discussion

According to the Fig. 2, three phonic band gaps (PBGs) are observed for the TM mode. They are located according to the interval mentioned in Table 1.

From the above diagram of the photonic band gap (Fig. 2), we obtain three band gaps in TM mode which is: a wide band which is located in this interval $0.2890 \leq a/\lambda \leq 0.4301$, a narrow band that locates in this range $0.7211 \leq a/\lambda \leq 0.7544$ and a very

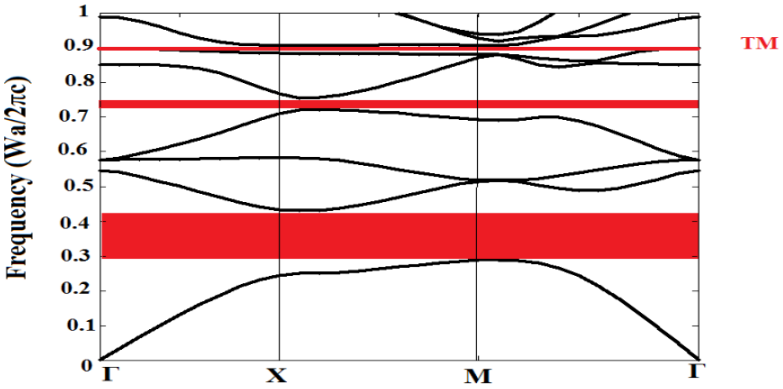

Fig. 2. The band structure for TM mode of the proposed sensor.

T a b l e 1. Three photonic band gaps of the TM mode with their intervals.

Mode TM	Interval λ [µm]
First PBG	[1.21599, 1.80968]
Second PBG	[0.693206, 0.72528]
Third PBG	[0.5778, 0.59499]

narrow band which is in the following range: $0.879 \leq a/\lambda \leq 0.905$. That is to say, the first band obtained is the widest wavelength λ which goes from 1.21599 up to 1.80968 µm. Then, we find the second narrow forbidden band where it covers a range of wavelength λ which gets along from 0.693206 to 0.72528 µm. And finally, we have the very narrow forbidden band which floats in a wavelength range between 0.5778 and 0.59499 µm. Knowing that these ranges were calculated this way, we have:

$$a/\lambda_n = f_n \tag{3}$$

$$f_n < a/\lambda_n < f \tag{4}$$

where a is the lattice constant, n is a natural number, λ is the wavelength, and f is the frequency.

Since the PBGs are respectively wide, narrow and very narrow, only the first PBG in TM mode is large enough to cover sufficient wavelengths for optical communication applications. In order to have a maximum of compatibility with the ranges of optical communication, we took a = 523 nm where the study will be in the range of 1.21599 µm < λ < 1.80968 µm in TM mode.

For this initial platform to be realized and operational, we first omitted along the Γ-X direction of the structure, a row of dielectric rods from the center in order to have an input port 1 and a port 2 of exit. Second, to design the rhombus shape, we removed 11×7 rods from the lattice of the initial structure. In addition, we made some changes

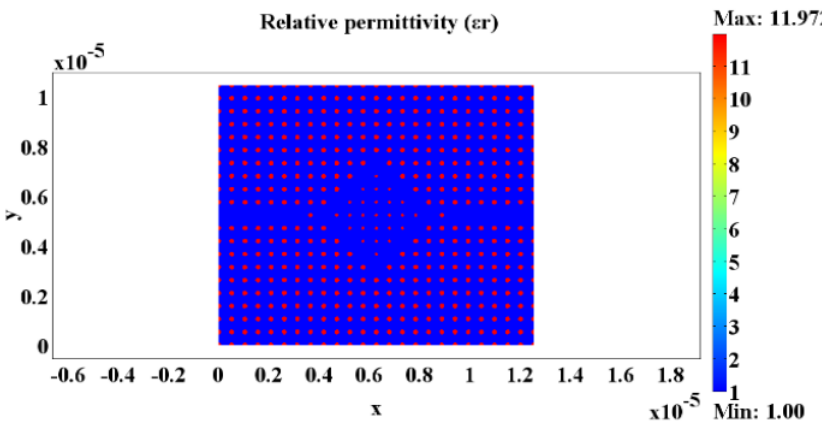

Fig. 3. (a) Dielectric permittivity and (b) mesh zoomed in the sensor study area

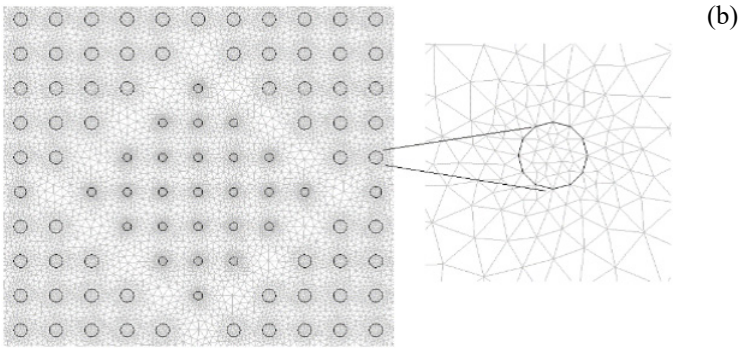

Fig. 3. Continued.

on the radius of some rods in the center of the rhombus in order to study the proposed sensor for glucose concentrations (Fig. 1(b)).

Figure 3(a), represents the distribution of the dielectric permittivity of silicon rods ($\varepsilon_{r(Si)} = 11.972$) immersed in air ($\varepsilon_{r(air)} = 1$) as well as (b), the mesh on the structure.

Figure 4 illustrates the electric field norm distribution at resonance, $\lambda = 1.3542$ µm (structure in the initial state). Then, we represented the distribution of the electric field norm E before and after changing the radius for different concentrations of glucose (10%, 20% and 60%) in water at the resonance wavelength, $\lambda = 1.55$ µm (see Fig. 5).

The next step of our work consists in modifying the radius in some rods which constitute the rhombus in the structure. The values of the radii which one touched are outside and inside the rhombus from where r_{out} becomes 0.08537 µm (radius in red) and r_{in} becomes 0.0637 µm (radius in green), see Fig. 1(b).

The final proposed structure (sensor) after modifying the radius of some of the rods is represented by two waveguides and a rhombus-shaped resonator and the overall size of the proposed sensor is 131.29 µm^2.

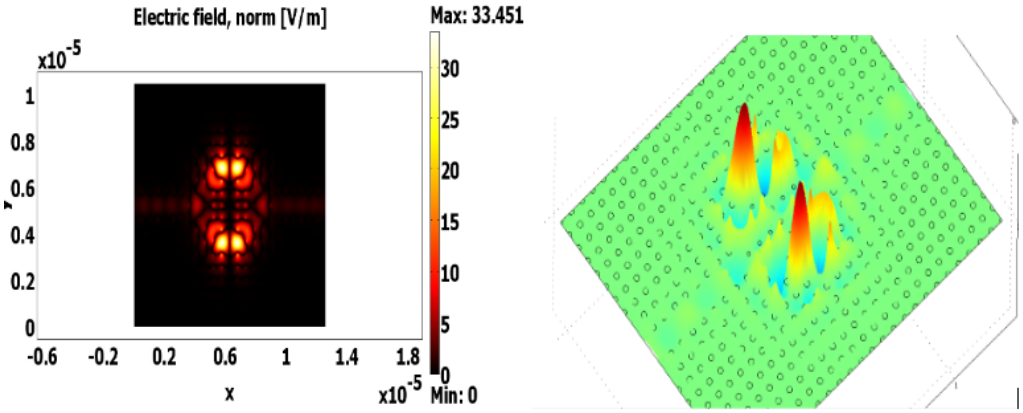

Fig. 4. Electric field norm distribution at the resonance, $\lambda = 1.3542$ µm.

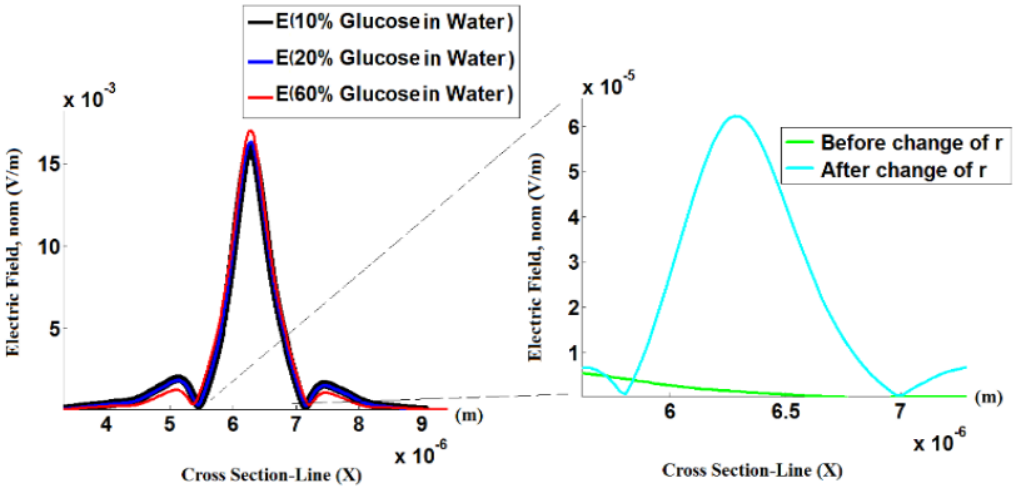

Fig. 5. The electric field norm distribution of the proposed sensor for three concentrations of glucose (10%, 20%, and 60%) in water at resonance wavelength, λ = 1.55 μm.

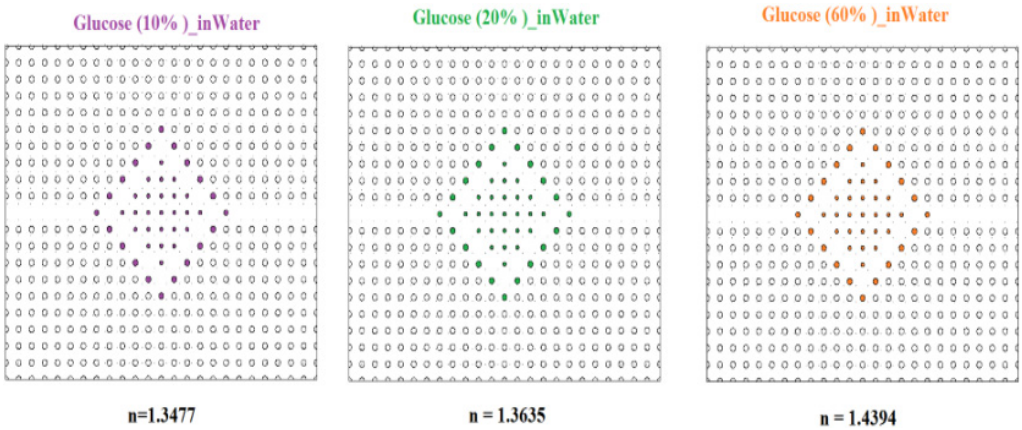

Fig. 6. The proposed sensor.

In order to explain our approach in this study, we presented three structures (see Fig. 6). Each structure will be modified according to the refractive index of each concentration of glucose introduced into the heart of the rhombus-shaped resonator. For example, the first structure has been modified by introducing a concentration of 10% glucose, hence the refractive index is 1.3477 (color move).

The second concentration of glucose introduced is 20% (see the resonator in green color) for a refractive index of 1.3635. Then, 60% glucose concentration was used in this rhombus for a refractive index, n = 1.4394 (orange color).

The results obtained by simulation showed that the electric field norm at resonance (λ = 1.55 μm) of Fig. 5 for the initial case (before changing the radius and introducing

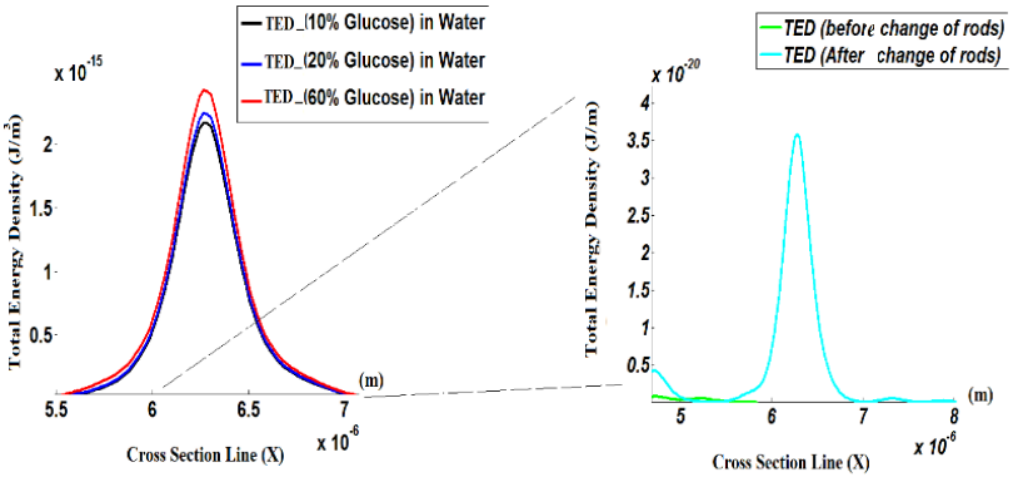

Fig. 7. The total energy density of the proposed sensor for three concentrations of glucose (10%, 20%, and 60%) in water at resonance wavelength, λ = 1.55 μm *versus* cross-section line.

the concentrations) is almost zero (= 1.362×10^{-6} V/m). Once the change takes place on the radius, we obtain a curve whose maximum is at 6.236×10^{-5} V/m. As soon as one begins to introduce the three concentrations of glucose (10%, 20% and 60%) into the rhombus-shaped resonator, one notices that the three new curves obtained have reached the maximum. These maximums are 17.01×10^{-3}, 16.3×10^{-3}, and 16×10^{-3} V/m for water glucose concentrations of 60%, 20%, and 10%, respectively, which coincide with the cut line at 6.286 μm. This can well explain the influence of the radius of the rod r on one side and on the other side of the refractive index at each introduced glucose concentration, on the maximum level of the norm intensity of the electric field which can be can reached.

In addition, another result that could be extracted is that of the total energy density (TED) before (and after) change of radius and without consultation as well as after the change of radius with the presence of the three concentrations of chosen glucose (Fig. 7). Therefore, the total energy density of the structure in the initial state is almost zero (green curve). Once the modifications are made to the radius of the rods that form the rhombus, a curve is observed with a maximum total energy density of 3.577×10^{-20} J/m^3 (cyan curve). Similarly, as soon as the first concentration of glucose at 10% is introduced, the curve changes and reaches a maximum density of 2.172×10^{-15} J/m^3 (black curve). The same goes for the concentrations of 20% and 60% which reach maximum total energy densities of 2.245×10^{-15} J/m^3 (blue curve) and 2.426×10^{-16} J/m^3 (red curve), respectively.

After the study of the TED, we illustrated the power flow norm (PFN), withits maximums in Table 2.

From Fig. 8, the variations in the maximums of the power flow norm (PFN) before (after) and in the presence of the concentrations of glucose in water on the structure were observed. According to Table 2, the power is almost zero ($\approx 3.483\times10^{-19}$ W/m^2)

T a b l e 2. The maximum power flow norm (PFN) before and after changing the radius of the rods and after the injection of the concentrations of glucose in the water.

	Before changing rods	After changing rods	Glucose (10%) in water	Glucose (20%) in water	Glucose (60%) in water
Max of power flow norm [W/m^2]	3.483×10^{-19}	2.261×10^{-15}	7.152×10^{-9}	7.853×10^{-9}	1.063×10^{-8}

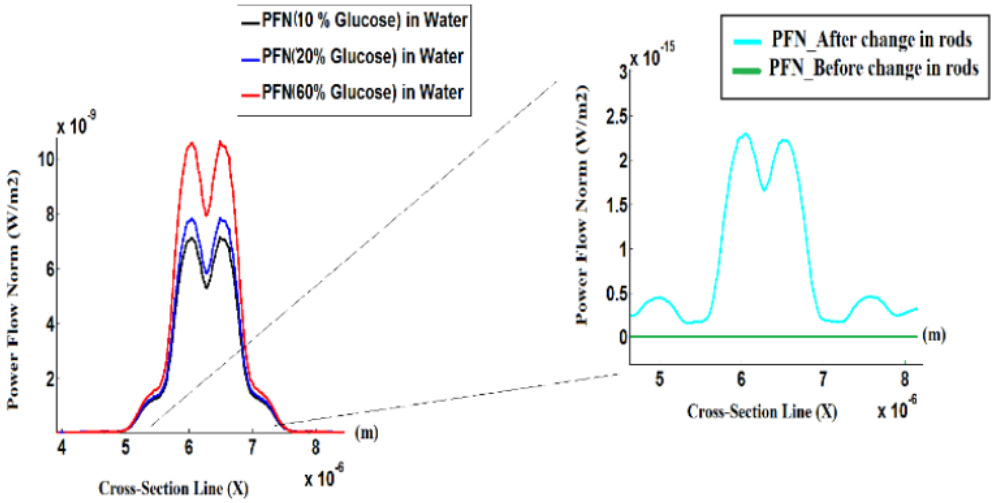

Fig. 8. The power flow norm distribution of the proposed sensor for three concentrations of glucose (10%, 20%, and 60%,) in water at resonance wavelength, λ = 1.55 μm *versus* cross-section line.

when the structure is in the initial state where the refractive index of rods is 3.46 (green curve). It begins to appear once the rods that form the rhombus change (cyan curve) where there is an increase to the maximum of PFN ≈ 2.261×10^{-15} W/m^2. As soon as the heart of the structure (rhombus) is replaced by 60% glucose (red curve) with a refractive index of 1.3477, the structure becomes sensitive and gives a maximum of 10.63×10^{-8} W/m^2. Once the concentration is divided by 3, *i.e.*, 20% (blue curve) for a refractive index n = 1.3635, there is a decrease in the maximum power which tends towards 0.7853×10^{-8} W/m^2. On the other hand, for a glucose concentration of 10% with a refractive index n = 1.4394 (black color), we notice there is a small decrease on the maximum of the power flow norm for a value of 0.7152×10^{-9} W/m^2. This gives us an insight into the impact and influence of the radius r and the concentration of glucose in water on the structure for the different doses used which can reach different maximums along the path from port 1 to the output of port 2. Knowing that the peaks of these curves intersect on the same line at 6.266 μm, we have:

The last parameter that we treated is the transmission according to the wavelength, see Fig. 9.

From this Fig. 9, the transmission is illustrated in dB. The results obtained show that the concentration of glucose at 10% (n = 1.3477) reaches a transmission value of

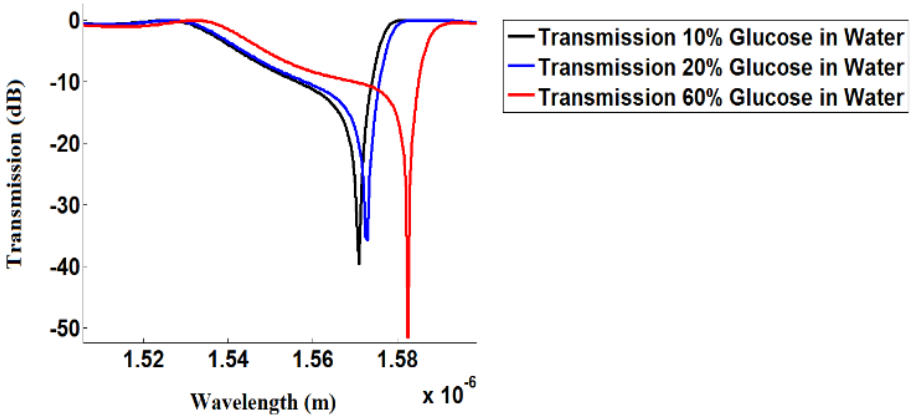

Fig. 9. Transmission for different concentrations of glucose with 10%, 20% and 60% *versus* wavelength.

–39.7 dB for a wavelength of 1.571 μm (curve in black) and the concentration of glucose at 20% (n = 1.3635) reaches the value of –35.78 dB at the wavelength of 1.573 μm (curve in blue). In addition, for the 60% glucose concentration where n = 1.4394 (red curve), the transmission reaches a value of –51.57 dB at a wavelength of 1.583 μm. This small wavelength shift for different concentrations of glucose in water proposed is 10 nm between 20% and 60%, 2 nm between 10% and 20% and 12 nm between 10% and 60% concentration. This difference in transmission and wavelength λ is due to the refractive index n which varies from one concentration of glucose to another.

Figure 10 summarizes the results obtained from the two curves which are the total energy density and the power flow norm as a function of the refractive index of the glucose concentrations used at 10%, 20% and 60% for the proposed biochip. It is noted

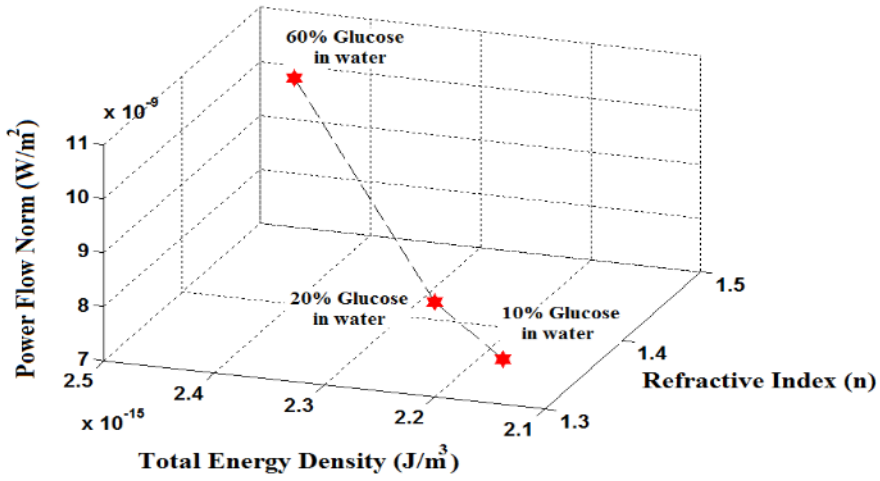

Fig. 10. The power flow norm and the total energy density versus refractive index of glucose concentration (10%, 20% and 60%) in water.

that the power flow norm and the total energy density increase together with the increase in glucose in the water for the concentrations of 10%, 20% and 60% hence their refractive index 1.3477, 1.3635 and 1.4394, respectively. Knowing that in the absence of glucose concentrations in the structure (initial state), the power and the energy density are almost zero.

This almost linearity obtained shows how the parameters r and n are very important for the sensitivity of the sensor that is proposed.

One of the important parameters for our sensor is the sensitivity. Sensitivity is defined as the level of a change in signal flow at a sensor in response to a change in refractive index of a glucose concentration. It is defined as follows:

$$S = \Delta\lambda/\Delta n \tag{5}$$

where $\Delta\lambda$ is the transmission spectrum displacement and Δn is the refractive index changes.

From Table 3, we could display the Fig. 11. This figure represents different glucose concentration solutions offered at 10%, 20% and 60% whose refractive index is 1.3477, 1.3635 and 1.4394, respectively.

These concentrations are used to determine the sensitivity S of the sensor which comprises a resonator in the shape of a rhomboid. Increasing the concentration with the refractive index n for each solution caused the resonance peaks λ_{res} in the spectra

T a b l e 3. Sensitivity S and resonance wavelength λ_{res} as a function of proposed refractive indices of glucose.

	n	λ_{res} [nm]	S [nm/RIU]
Glucose (10%)	1.3477	1571	–
Glucose (20%)	1.3635	1573	127
Glucose (60%)	1.4394	1583	132

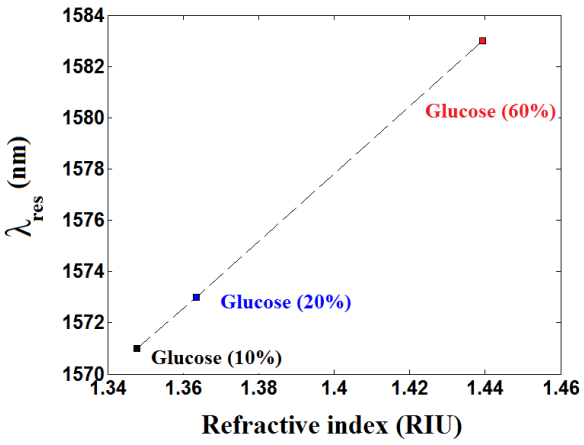

Fig. 11. Resonant wavelength plotted as a function of refractive index n.

to shift to longer wavelengths (Fig. 11). The obtained offset $\Delta\lambda$ can in a small range of refractive indices Δn be approximated by a linear fit. The linearity of Fig. 11 shows a sensitivity of 132 nm/RIU for the highest sensitivity peak.

4. Conclusions

In this work, we proposed the study and the simulation of glucose concentrations through a biochip based on two-dimensional photonic crystals. In order to detect these concentrations for doses of 10%, 20% and 60%, we proposed a structure composed of two waveguides which sandwich a rhombus-shaped resonator that is on a horizontal line. This so-called chip structure is made from silicon (Si) rods immersed in air. The area of this structure is 114 μm^2. The core of our numerical results are obtained thanks to the two-simulation software MATLAB and COMSOL. They are able to help extract the photonic band gap (BIP), electric field norm (E), power flow norm (PFN), total energy density (TED), transmission (T) and deduce the sensitivity by using the resonant wavelength curve which is plotted as a function of refractive index (n). These numerical results give a clear observation on the behavior of this platform in the presence of the proposed glucose concentrations and the important role played by the radius r and the refractive index n in each material used. These two parameters are relevant factors for detection. Such a device, which makes it possible to measure the concentrations of glucose in human saliva, is applicable to the monitoring of diabetes. It can also be applied in the environment as well as the measurement of biological substances.

References

[1] Robinson S., Dhanlaksmi N., *Photonic crystal based biosensor for the detection of glucose concentration in urine*, Photonic Sensors **7**, 2017: 11-19. https://doi.org/10.1007/s13320-016-0347-3

[2] Ansari J.N., Gowre S.C., Sonth M.V., Gadgay B., Roy A.S., *Photonic nano dielectric crystal cavity with infiltrated biosamples for refractive index sensing application*, Integrated Ferroelectrics **213**(1), 2021: 93-102. https://doi.org/10.1080/10584587.2020.1859827

[3] Maleki M.J., Soroosh M., Mir A., *Improving the performance of 2-To-4 optical decoders based on photonic crystal structures*, Crystals **9**(12), 2019: 635. https://doi.org/10.3390/cryst9120635

[4] Rezaei M.H., Yavari M.H., *High-sensitive symmetric Fano optical cavity sensor for refractive index detection based on photonic crystal structure*, 29th Iranian Conference on Electrical Engineering (ICEE), Tehran, Iran, 2021: 18-22. https://doi.org/10.1109/ICEE52715.2021.9544343

[5] Haddadan F., Soroosh M., Alaei-Sheini N., *Designing an electro-optical encoder based on photonic crystals using the graphene–Al_2O_3 stacks*, Applied Optics **59**(7), 2020: 2179-2185. https://doi.org/10.1364/AO.386248

[6] Zhao Y., Vora K.H., vom Bögel G., Seidl K., Weidenmüller J., *Design and simulation of a photonic crystal resonator as a biosensor for point-of-care applications*, tm - Technisches Messen **87**(7-8), 2020: 470-476. https://doi.org/10.1515/teme-2019-0127

[7] Kamrunnahar Q.M., Haider F., Aoni R.A., Mou J.R., Shifa S., Begum F., Abdul-Rashid H.A., Ahmed R., *Plasmonic micro-channel assisted photonic crystal fiber based highly sensitive sensor for multi-analyte detection*, Nanomaterials **12**(9), 2022: 1444. https://doi.org/10.3390/nano12091444

[8] Azizpour M.R.J., Soroosh M., Dalvand M., Seifi-Kavian Y., *All-optical ultra-fast graphene-photonic crystal switch*, Crystals **9**(9), 2019: 461. https://doi.org/10.3390/cryst9090461

[9] SERAJ Z., SOROOSH M., ALAEI-SHEINI N., *Ultra-compact ultra-fast 1-bit comparator based on a two-dimensional nonlinear photonic crystal structure*, Applied Optics **59**(3), 2020: 811-816. https://doi.org/10.1364/AO.374428

[10] ZAMANI N.D.M., NAWI M.N., BERHANUDDIN D.D., MAJLIS B.Y., MD. ZAIN A.R., *Design of 2D GaN photonic crystal based on hole displacement for L3 cavity*, Nanomaterials and Nanotechnology **10**, 2020: 1-5. https://doi.org/10.1177/1847980420966887

[11] SÜNNER T., STICHEL T., KWON S.-H., SCHLERETH T.W., HÖFLING S., KAMP M., FORCHEL A., *Photonic crystal cavity based gas sensor*, Applied Physics Letters **92**(26), 2008: 261112. https://doi.org/10.1063/1.2955523

[12] WU D.K.C., KUHLMEY B.T., EGGLETON B.J., *Ultrasensitive photonic crystal fiber refractive index sensor*, Optics Letters **34**(3), 2009: 322-324. https://doi.org/10.1364/OL.34.000322

[13] RADHOUENE M., CHHIPA M. K., NAJJAR M., ROBISON S., SUTHAR B., *Novel design of ring resonator based temperature sensor using photonics technology*, Photonic Sensors **7**, 2017: 311-316. https://doi.org/10.1007/s13320-017-0443-z

[14] ARUNKUMAR R., SUGANYA T., ROBINSON S., *Design and analysis of photonic crystal elliptical ring resonator based pressure sensor*, International Journal of Photonics and Optical Technology **3**(1), 2017: 30-33.

[15] SREENIVASULU T., KOLLI V.R., ANUSREE K., YADUNATH T.R., BADRINARAYANA T., SRINIVAS T., HEGDE G., MOHAN S., *Photonic crystal based force sensor on silicon microcantilever*, [In] *2015 IEEE SENSORS*, Busan, Korea (South), India, 2015. https://doi.org/10.1109/ICSENS.2015.7370225

[16] ROBINSON S., SHANTHI K.V., *Analysis of protein concentration based on photonic crystal ring resonator*, International Journal of Optics and Photonics (IJOP) **10**(2), 2016: 123-130. https://doi.org/10.18869/acadpub.ijop.10.2.123

[17] GHOUMAZI M., HAMEURLAIN M., *Study and simulation of a sensor based on 2D photonic crystals for the detection of aromatic compounds: C_6H_5I, C_6H_5F and C_6H_5Cl*, Annales de Chimie - Science des Matériaux **45**(4), 2021: 335-339. https://doi.org/10.18280/acsm.450409

[18] GHOUMAZI M., BELLA M., HAMEURLAIN M., *Designing of a novel nanophotonic structure based on 2D photonic crystals for the detection of different materials*, Mathematical Modelling of Engineering Problems **9**(1), 2022: 19-26. https://doi.org/10.18280/mmep.090103

[19] KHANI S., HAYATI M., *Optical biosensors using plasmonic and photonic crystal band-gap structures for the detection of basal cell cancer*, Scientific Reports **12**, 2022: 5246. https://doi.org/10.1038/s41598-022-09213-w

[20] LEE M., FAUCHET P.M., *Two-dimensional silicon photonic crystal based biosensing platform for protein detection*, Optics Express **15**(8), 2007: 4530-4535. https://doi.org/10.1364/OE.15.004530

[21] DI FALCO A., O'FAOLAIN L., KRAUSS T.F., *Chemical sensing in slotted photonic crystal heterostructure cavities*, Applied Physics Letters **94**(6), 2009: 063503. https://doi.org/10.1063/1.3079671

[22] CHEN L., MORGAN K. A., ALZAIDY G. A., HUANG C-C., HO Y-L.D., TAVERNE M.P.C., ZHENG X., REN Z., FENG Z., ZEIMPEKIS I., HEWAK D.W., RARITY J.G., *Observation of complete photonic bandgap in low refractive index contrast inverse rod-connected diamond structured chalcogenides*, ACS Photonics **6**(5), 2019: 1248-1254. https://doi.org/10.1021/acsphotonics.9b00184

[23] SCHWARTZ B.T., PIESTUN R., *Dynamic properties of photonic crystals and their effective refractive index*, Journal of the Optical Society of America B **22**(9), 2005: 2018-2026. https://doi.org/10.1364/JOSAB.22.002018

[24] SOLTANI O., FRANCOEUR S., KANZARI M., *Superconductor-based quaternary photonic crystals for high sensitivity temperature sensing*, Chinese Journal of Physics **77**, 2022: 176-188. https://doi.org/10.1016/j.cjph.2022.02.007

[25] AGARWAL A., MUDGAL N., SAHU S., SINGH G., BHATNAGAR S.K., *Design of a nanocavity photonic crystal structure for biosensing application*, [In] Tiwari M., Maddila R.K., Garg A.K., Kumar A., Yupapin P. [Eds], *Optical and Wireless Technologies*, Lecture Notes in Electrical Engineering, Vol. 771, Springer, Singapore, 2022: 321-330.

[26] Chou Chao C.-T., Chou Chau Y.-F., Chen S.-H., Huang H.J., Lim C.M., Kooh M.R.R., Thotagamuge R., Chiang H-P., *Ultrahigh sensitivity of a plasmonic pressure sensor with a compact size*, Nanomaterials **11**(11), 2021: 3147. https://doi.org/10.3390/nano11113147

[27] Troia B., Paolicelli A., De Leonardis F., Passaro V.M.N., *Photonic crystals for optical sensing: A review*, [In] *Advances in Photonic Crystals*, IntechOpen, 2013.

[28] Petrova I., Konopsky V., Nabiev I., Sukhanova A., *Label-free flow multiplex biosensing via photonic crystal surface mode detection*, Scientific Reports **9**, 2019: 8745. https://doi.org/10.1038/s41598-019-45166-3

[29] Viswanathan B., Rajesh A., Jeyalakshmi C., Abinaya S., Deepika J., Dharini D., Gajasree S., *Design of 6-channel optical demultiplexer/coupler using photonic crystal for IFoF in 5G networks*, Optical and Quantum Electronics **53**, 2021: 444. https://doi.org/10.1007/s11082-021-03097-2

[30] Shirdely M., Mansouri-Birjandi M.A., *Photonic crystal all-optical switch based on a nonlinear cavity*, Optik **127**(8), 2016: 3955-3958. https://doi.org/10.1016/j.ijleo.2016.01.114

[31] Mandal S., Bose M.K., Bose C., *Generalized scheme for coupling length reduction in photonic crystal based directional coupler designed with square lattice of dielectric rods in air background*, Optik **198**, 2019: 163273. https://doi.org/10.1016/j.ijleo.2019.163273

[32] Jindal P., Geetanjali, Gupta I., Kaur H.J., *Photonic crystal power splitter with linear waveguides in a low dielectric-index material*, 5th International Conference on Electronics, Communication and Aerospace Technology (ICECA), 2021: 312-319. https://doi.org/10.1109/ICECA52323.2021.9675986

[33] Caballero L.P., Povinelli M. L., Ramirez J.C., Guimarães P.S.S., Vilela Neto O.P., *Photonic crystal integrated logic gates and circuits*, Optics Express **30**(2), 2022: 1976-1993. https://doi.org/10.1364/OE.444714

[34] Wang J., Huangfu L., Chen H., *Design of compact polarization-insensitive multimode interference triplexer*, Journal of Modern Optics **68**(9), 2021: 496-506. https://doi.org/10.1080/09500340.2021.1924887

[35] Hodson T., Miao B., Chen C., Sharkawy A., Prather D., *Silicon based photonic crystal electro-optic modulator utilizing the plasma dispersion effect*, [In] *2007 Conference on Lasers and Electro-Optics (CLEO)*, Baltimore, MD, USA, 2007: 1-2. https://doi.org/10.1109/CLEO.2007.4452748

[36] Bazian M., *Photonic crystal add–drop filter: A review on principles and applications*, Photonic Network Communications **41**, 2021: 57-77. https://doi.org/10.1007/s11107-020-00907-7

[37] Seifouri M., Fallahi V., Olyaee S., *Ultra-high-Q optical filter based on photonic crystal ring resonator*, Photonic Network Communications **35**, 2018: 225–230. https://doi.org/10.1007/s11107-017-0732-x

[38] Ghoumazi M., Hocini A., *Photonic crystal based bio-sensor detection in nanophotonic structure using FEM method*, International Journal of Sensors, Wireless Communications and Control **11**(2), 2021: 216-224. https://doi.org/10.2174/2210327910666191218125109

[39] Baker J.E., Sriram R., Miller B.L., *Two-dimensional photonic crystals for sensitive microscale chemical and biochemical sensing*, Lab Chip **15**(4), 2015: 971-990. https://doi.org/10.1039/C4LC01208A

[40] Pitruzzello G., Krauss T.F., *Photonic crystal resonances for sensing and imaging*, Journal of Optics **20**(7), 2018: 073004. https://doi.org/10.1088/2040-8986/aac75b

[41] Fu H.-W., Zhao H., Qiao X.-G., Li Y., Zhao D.-Z., Yong Z., *Study on a novel photonic crystal temperature sensor*, Optoelectronics Letters **7**, 2011: 419-422. https://doi.org/10.1007/s11801-011-0065-4

[42] Sinibaldi A., *Cancer biomarker detection with photonic crystals-based biosensors: An overview*, Journal of Lightwave Technology **39**(12), 2021: 3871-3881.

[43] Olyaee S., Mohsenirad H., Mohebzadeh-Bahabady A., *Photonic crystal chemical/biochemical sensors*, [In] *Progresses in Chemical Sensor*, IntechOpen, London, United Kingdom, 2016.

[44] Rodriguez-Esquerre V.F., Koshiba M., Hernandez-Figueroa H.E., *Finite-element analysis of photonic crystal cavities: time and frequency domains*, Journal of Lightwave Technology **23**(3), 2005: 1514-1521.

[45] XIAO S., SHEN L., HE S., *A plane-wave expansion method based on the effective medium theory for calculating the band structure of a two-dimensional photonic crystal*, Physics Letters A **313**(1-2), 2003: 132-138. https://doi.org/10.1016/S0375-9601(03)00690-X

[46] ANDONEGUI I., GARCIA-ADEVA A.J., *The finite element method applied to the study of two-dimensional photonic crystals and resonant cavities*, Optics Express **21**(4), 2013: 4072-4092. https://doi.org/10.1364/OE.21.004072

[47] PAINTER O., VUČKOVIĆ J., SCHERER A., *Defect modes of a two-dimensional photonic crystal in an optically thin dielectric slab*, Journal of the Optical Society of America B **16**(2), 1999: 275-285. https://doi.org/10.1364/JOSAB.16.000275

[48] CHUPRADIT S., ASHFAQ S., BOKOV D., SUKSATAN W., JALIL A.T., ALANAZI A.M., SILLANPAA M., *Ultra -sensitive biosensor with simultaneous detection (of cancer and diabetes) and analysis of deformation effects on dielectric rods in optical microstructure*, Coatings **11**(12), 2021: 1564. https://doi.org/10.3390/coatings11121564

[49] ROSTAMIAN A., MADADI-KANDJANI E., DALIR H., SORGER V.J., CHEN R.T., *Towards lab-on-chip ultrasensitive ethanol detection using photonic crystal waveguide operating in the mid-infrared*, Nanophotonics **10**(6), 2021: 1675-1682. https://doi.org/10.1515/nanoph-2020-0576

Received December 27, 2022
in revised form March 25, 2023